



# A New Fiber Detection Method for LAMOST Based on the Front-illuminated Method

Ming Zhou<sup>1,2</sup>, Yong Zhang<sup>3</sup>, Guanru Lv<sup>1</sup>, Jian Li<sup>1</sup>, Zengxiang Zhou<sup>4</sup> , Zhigang Liu<sup>4</sup>, Jianping Wang<sup>4</sup>, Zhongrui Bai<sup>1</sup>, Yuan Tian<sup>1</sup>, Mengxin Wang<sup>1</sup>, Shuqing Wang<sup>1</sup>, Hongzhuan Hu<sup>4</sup>, Chao Zhai<sup>4</sup>, Jiaru Chu<sup>4</sup>, Zhijie Han<sup>1</sup>, Mingxu Liu<sup>1</sup>, Yiqiao Dong<sup>1</sup>, Hailong Yuan<sup>1</sup>, Yongheng Zhao<sup>1</sup>, Yaoquan Chu<sup>4</sup>, and Haotong Zhang<sup>1</sup>

<sup>1</sup> Key Laboratory of Optical Astronomy, National Astronomical Observatories, Chinese Academy of Sciences, Beijing 100101, China; [htzhang@bao.ac.cn](mailto:htzhang@bao.ac.cn)

<sup>2</sup> University of Chinese Academy of Sciences, Beijing 100049, China

<sup>3</sup> National Astronomical Observatories/Nanjing Institute of Astronomical Optics & Technology, Chinese Academy of Sciences, Nanjing 210042, China  
[yzh@niaot.ac.cn](mailto:yzh@niaot.ac.cn)

<sup>4</sup> University of Science and Technology of China, Hefei 230026, China

Received 2022 March 23; revised 2022 April 7; accepted 2022 April 12; published 2022 May 20

## Abstract

The double revolving fiber positioning technology is one of the key technologies for the success of the Large Sky Area Multi-Object Fiber Spectroscopic Telescope (LAMOST). The accuracy of fiber positioning will directly affect the observation efficiency of LAMOST. To achieve higher fiber positioning accuracy, the original open-loop controlled fiber positioning system urgently needs to be upgraded into a closed-loop control system. The fiber detection is the most important part of the closed-loop controlled fiber positioning system. The back-illuminated detection method is usually used to detect the fiber position by directly detecting the light spot generated at the fiber end in the multi-fiber spectral surveys. In this paper, we introduce a new method to measure the fiber position based on the image of the front-illuminated LAMOST focal plane. The front-illuminated image does not require lighting devices inside the spectrograph, and it could reduce the instability and light pollution in the spectrograph end. Our method measures the fiber position by fitting the profile of the fiber pinhole with a 2D Gaussian function. A series of tests show that the relative position measurement precision of the front-illuminated method is about  $0''.12$ , and the method could have the same accuracy as the back-illuminated method once the system bias is calibrated by a simple radial correction function. The required fiber positioning accuracy of LAMOST is  $0''.4$ , and the new method satisfies the requirement of LAMOST fiber detection accuracy and could be used in the closed-loop fiber control system.

*Key words:* techniques: image processing – methods: data analysis – instrumentation: detectors

## 1. Introduction

Multi-object fiber surveys use a large number of fibers to observe multiple objects simultaneously. Fiber positioning robots are commonly adopted in modern large-scale multifiber spectral surveys to save both manpower and fiber positioning time. Parallel controllable fiber positioning system (Xing et al. 1998) with double revolving fiber positioning unit (FPU) was first realized in the Large Sky Area Multi-Object Fiber Spectroscopic Telescope (LAMOST) (Cui et al. 2012), which could simultaneously position 4000 fibers within 0.4 arcsec accuracy in 10 minutes. Subsequent surveys, such as the Dark Energy Spectroscopic Instrument (DESI) (Schubnell et al. 2016), the Multi-Object Optical and Near-infrared Spectrograph (MOONS) (Montgomery et al. 2016) and the Prime Focus Spectrograph (PFS) (Fisher et al. 2014) for Subaru telescope all use LAMOST style fiber positioning system for fiber positioning.

The new surveys are usually equipped fiber position monitoring camera to achieve closed-loop control of the fiber

position, e.g., PFS (Wang et al. 2016), MOONS (Drass et al. 2016) and DESI (Baltay et al. 2019). LAMOST currently uses an open-loop controlled fiber positioning system. To ensure the positioning accuracy in the open-loop system, the FPUs must return to a pre-calibrated home position before going to a new position. This step consumes about half of the time in fiber positioning. The fiber positioning accuracy of the open-loop control system is limited by the robot accuracy and initial parameters of FPU (Zhou et al. 2021a). The LAMOST fiber positioning accuracy of the open-loop controlled system is better than 40 microns (0.4 arcsec) after system calibration (Liu et al. 2011) in the summer. However, collisions between adjacent FPUs due to occasional mechanical failures during long-term operation will eventually lead to the decline of fiber positioning accuracy and the damage of FPUs. In order to improve fiber positioning accuracy and reduce the reconfiguration time, the current fiber positioning system needs to be upgraded into a closed-loop control system. In a closed-loop fiber positioning system, the fiber position measured by the

fiber monitoring camera will be fed back to the control system. Based on the differences between the measured position and the expected position, the FPU will move accordingly and the required fiber positioning accuracy will be achieved after multiple iterations. Therefore, the key to implement a closed-loop control system is to accurately measure the fiber position.

The fiber detection in the multi-fiber spectral surveys usually use two methods of illumination: back-illuminated method (Wang et al. 2016; Hörler 2018; Baltay et al. 2019) and front-illuminated method (Drass et al. 2016). The back-illuminated method is a direct detection method. The fibers are illuminated from the spectrograph end, the other end of the fibers on the focal plane will produce a light spot which is then used to measure the fiber position. Surveys using the back-illuminated method include DESI and PFS. Front-illumination uses light to illuminate the FPUs on the focal plane, thus the structure of the FPU could be resolved (Zhou et al. 2021a). One can use the dedicated metrology targets on top of the FPU (as in MOONS) or the pinhole of the fiber end (as in this paper) to measure the fiber position.

To achieve the closed-loop controlled fiber positioning system, LAMOST is constructing the fiber detection system, both back-illuminated and front-illuminated methods can be used to detect the fiber. The LAMOST back-illumination system consists of a slit of LED bubbles which matches the fiber slit, and a device to move the LED slit in and out the light path. Compared with the front-illuminated method, the back-illuminated method usually has higher detection accuracy and is easier to implement. Yet the back-illumination system has several drawbacks (Zhou et al. 2021b): first, the mechanical device adds complexity of the system. The LED bubble slit has to move in and out light path during closed-loop control, which caused the instability due to the increased risk of mechanical errors. Second, the light inside the spectrograph adds risk of light pollution, especially the overwhelming photons may cause the CCD saturation and leaving residual electric charge hard to be erased. Third, the mechanical movement of the device adds more overhead time when observing. While the front-illumination system illuminates the mechanical structures of the FPU in front of the focal plane, both the pinhole of the fiber and the revolving arms could be resolved. The fiber is mounted in a pinhole of FPU, and the pinhole position in the image corresponds exactly to the fiber position after the correction of the light projection. Although the FPUs of LAMOST are not specifically designed for the front-illuminated detection, its mechanical features make it possible to use the front-illuminated method for fiber detection. In this paper, we propose a new front-illuminated detection method according to the structural characteristics of the FPU, which does not require additional metrology target on the FPU. The detection accuracy of our method is basically consistent with the back-illuminated method, which provides a new and reliable fiber detection technology for LAMOST.

The layout of this paper is as follows. The second section introduces our method based on the front-illuminated image. The third section presents results and the comparison with the back-illuminated method. Test results to verify the reliability and accuracy of our method are also demonstrated in this section. Discussion and summary are in the conclusion section.

## 2. Method

To achieve the closed-loop control system, LAMOST is constructing the fiber detection system, which detects the fiber position by acquiring the image of the focal plane through the fiber monitoring camera. This section presents the details of our new detection method based on the front-illuminated image captured by the fiber monitoring camera. The fiber is mounted in a pinhole of FPU with very tight tolerance (see Figure 2), and so we get the fiber position by detecting the pinhole using the front-illuminated image.

### 2.1. Front-illuminated Image

The fiber detection system (Zhao et al. 2018) of LAMOST is shown in Figure 1. The fiber units could be illuminated by the back-illuminated device that illuminates the fiber from the spectrograph or the front-illuminated device that illuminates the FPU in the front of the focal plane. Multiple cameras are placed off-axis around the primary mirror at distances about 20 m from the focal plane. Each camera consists of a 800 mm focal length lens and a  $7920 \times 6004$  pixels CMOS camera. The pixel size of the camera is  $4.6 \times 4.6 \mu\text{m}$ , corresponding to  $115 \mu\text{m}$  on the focal plane or  $1''.18$  in the sky. Each camera covers a part of the focal plane and the results from different camera will be combined. As a preliminary test of the method, only one camera is used in this paper.

The front-illuminated image captured by the camera facing the lower left part of the focal plane is shown in the left panel of Figure 2. A single FPU is amplified in the right panel, where the white circular disk is the ceramic ferrule/holder that hold the fiber in the pinhole (central dark spot), and the diameters of ceramic ferrule and pinhole are about 2.5 mm and  $384 \mu\text{m}$ , respectively. The light will be diffusely reflected by the fiber ferrule and the pinhole will be dark under front illumination.

### 2.2. Pinhole Extraction

The pinhole inside the fiber holder is where the fiber mounted. Rather than detecting the dark pinhole directly, it is much easier to detect the circular disk of the fiber holder first, then extract the pinhole inside the ceramic ferrule. The detection process of the fiber holder is shown in Figure 3. First, a  $3 \times 3$  filter is used to remove the noise of the image, then the canny operator (Duan et al. 2005) is used to depict the edge information of the FPU, as shown in the middle panel. Finally, the Hough transform algorithm (Zhu & Zhang 2008) is

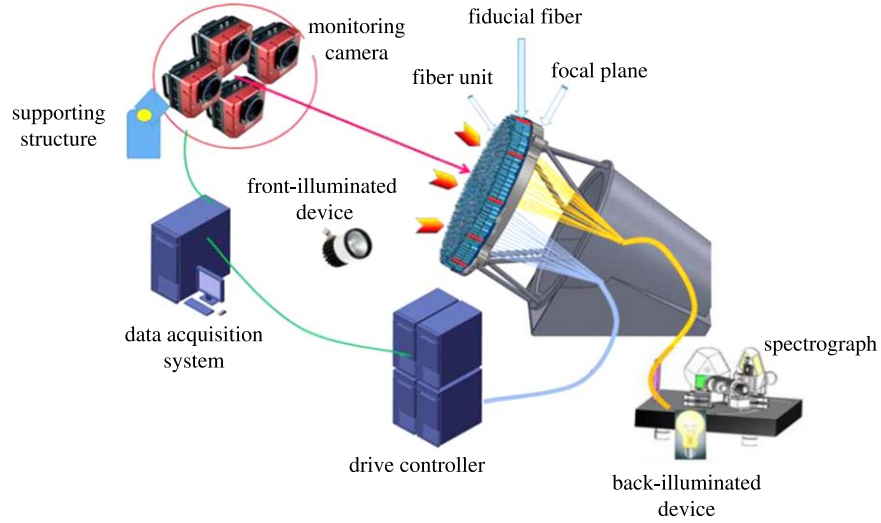


**Figure 1.** Schematic diagram of the fiber monitoring camera system for LAMOST. The fiber unit is illuminated by the front-illuminated and back-illuminated devices. The fiber monitoring cameras detect the fiber position using the image of the fiber unit in real time and feed the information back to the FPU control system.

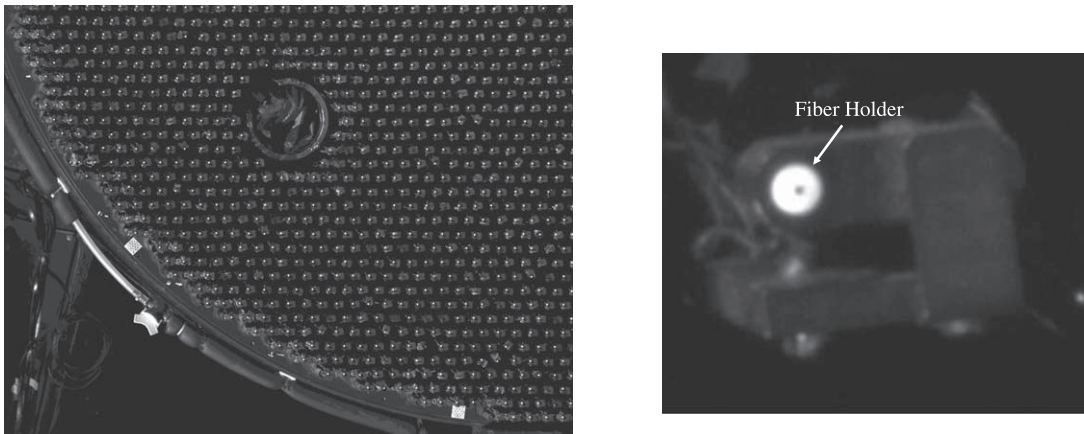


**Figure 2.** Front-illuminated image of the lower left part of the focal plane captured by a camera. The left panel shows the whole image. The right panel is a single FPU trimmed from the left image, where the black spot inside the fiber holder is a pinhole used to mount the fiber.

applied to the binarized image from the previous step. By constraining the size and the number of consecutive points of the circle, the ceramic ferrule could be successfully detected, but with not high enough accuracy ( $0.2''$ ) to describe the fiber position due to the detection error of circular fiber holder caused by illumination and projection errors, as in Figure 3(c).

The dark pinhole in the front-illuminated image can be used to detect the fiber position. To accurately extract the pinhole, we cut a square inscribed in the circular fiber holder. The image of the pinhole extracted from the front-illuminated image is shown in Figure 4(a), where the black spot in the image corresponds to the pinhole inside the fiber holder. Then the extracted image is inverted for changing them into conventional bright spots and then treating them in the usual way of

subsequent processing, and the inverted gray values are expressed as:

$$\text{gray}_{\text{inv}} = \text{gray}_{\text{max}} - \text{gray}, \quad (1)$$

where the  $\text{gray}_{\text{max}}$  is the maximum gray value of the image. Since the image is read out in 12-bit integer,  $\text{gray}_{\text{max}} = 4095$ . 3D plot of the inverted pinhole is shown in Figure 4(b), which is approximate Gaussian distribution.

### 2.3. Fiber Position Measurement

Methods such as Gaussian distribution fitting, gray scale centroid and average of perimeter (Shortis et al. 1994) could be applied to calculate the positions of the discrete target images. As is shown in Figure 4(b), the background in the image is

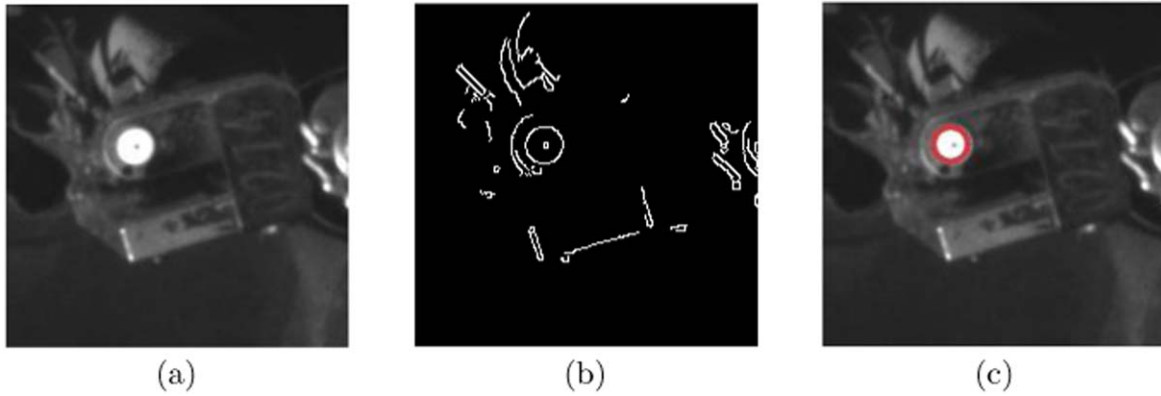


**Figure 3.** The detection process of the fiber holder. (a) The front-illuminated image of a single FPU. (b) The edge of the FPU detected by canny operator. (c): The ceramic fiber holder detected by Hough transform, as indicated by the red circle.

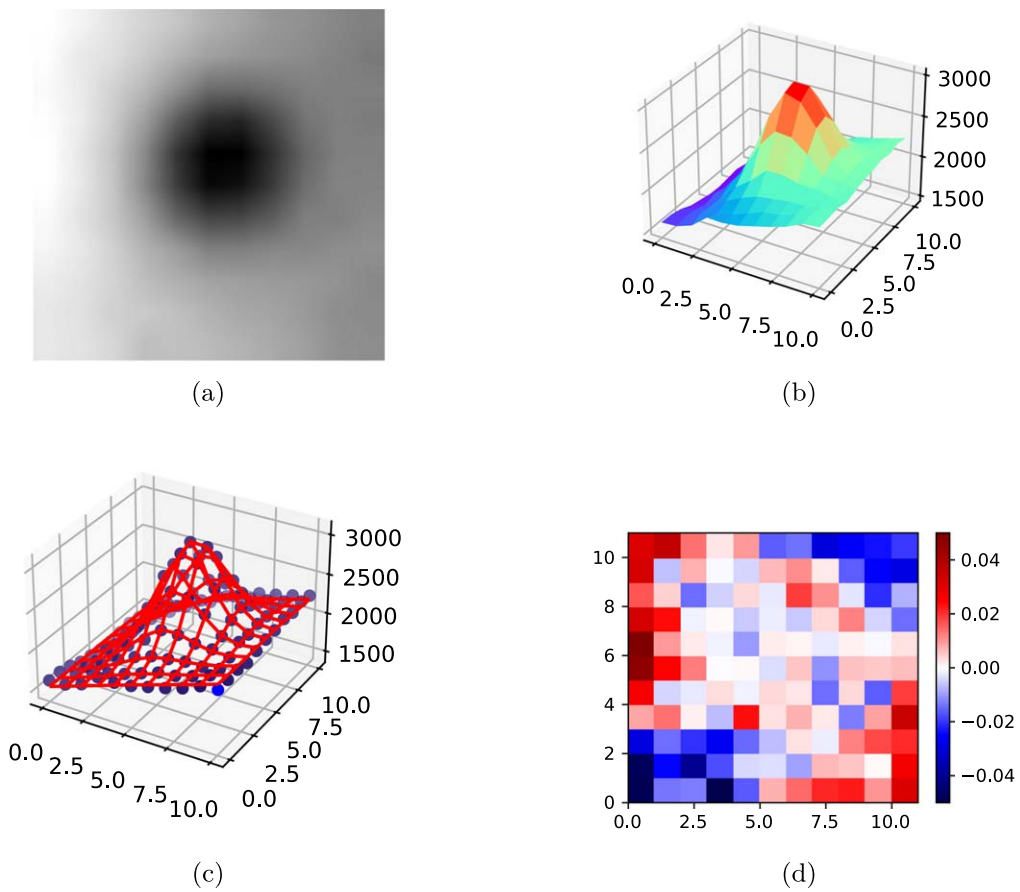


**Figure 4.** Extraction and location of the pinhole. (a) A pinhole inside the fiber holder extracted from the front-illuminated image. (b) Distribution of gray values of the pinhole after inversion. (c) Gaussian fitting of the pinhole with Equation (2), where the blue dot is the gray values as in (b), and red grids are the fitting result. (d) Relative residual of the Gaussian fitting.

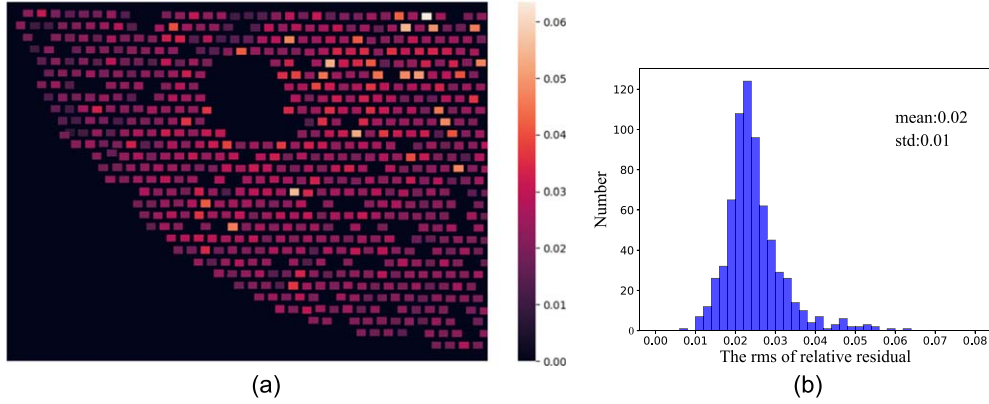


**Figure 5.** (a) The rms of the relative residual of each FPU fitting with Equation (2), where each rectangle represents an FPU. The central big blank region comes from the unusual FPU mainly caused by the front lighting and FPU itself. (b) The statistical results of the rms of the relative residual fitting, and the rms of almost all FPU is less than 0.04.

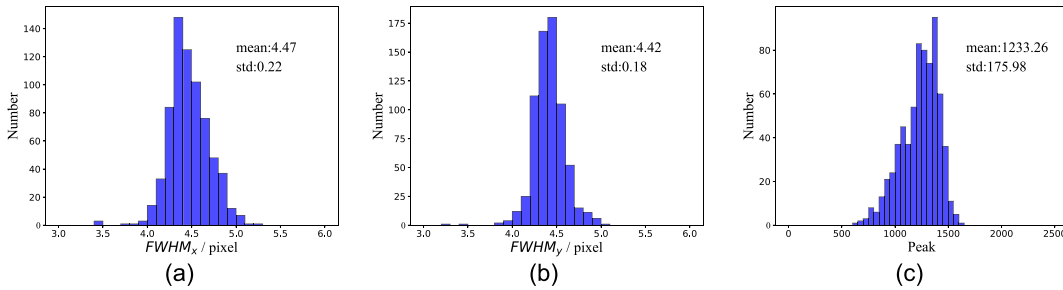


**Figure 6.** The distribution of width and peak of pinhole after subtracting the background. The width of the light spot in the horizontal and vertical directions is basically the same, indicating that the profile is symmetrical in these two directions, and the signal intensity is sufficient to accurately calculate the spot position.

uneven due to the uneven illumination for each FPU. The centroid or average perimeter method will be biased when the background is not homogeneously distributed as in this case. Therefore, the Gaussian fitting method that simultaneously fits the background and the pinhole profile is adopted,

$$g(x, y) = A * e^{-Q/2} + a * x + b * y + c,$$

$$Q = \frac{1}{1 - \rho^2} \left[ \left( \frac{x - \mu_x}{\sigma_x} \right)^2 + \left( \frac{y - \mu_y}{\sigma_y} \right)^2 + 2\rho \left( \frac{x - \mu_x}{\sigma_x} \right) \left( \frac{y - \mu_y}{\sigma_y} \right) \right] \quad (2)$$

Here  $g(x, y)$  is the gray value of the corresponding pixel  $(x, y)$ ,  $\mu_x$  and  $\mu_y$  are the fitted center of pinhole,  $\sigma_x$  and  $\sigma_y$  represent the width of the Gaussian profile,  $\rho$  is the correlation coefficient between  $x$  and  $y$ ,  $a$ ,  $b$  and  $c$  are the parameters describing the background plane. The fitting of a single pinhole is demonstrated in Figures 4(c)–(d). The method is applied to measure the position of each FPU in the image. Figure 5 shows the distribution of the rms of the relative residual for each FPU on

focal plane. As can be seen in Figures 4(d) and 5, the residuals of our Gaussian profile and the background fitting are only a few percent, and there is no obvious system tendency in residual image of Figure 5. The distribution of the FWHM of the Gaussian profile in the  $x$  and  $y$  directions, as well as the distribution of the peak of the Gaussian profile, are shown in Figures 6(a)–(c), respectively. The FWHM of fiber spot in the image is about 4.5 pixels in both horizontal and vertical directions, which shows that the front illumination in two directions is basically symmetrical. About 90% of the peak values of the pinhole images after removing background are higher than 1000, which is sufficient to accurately calculate the spot position.

### 3. Results and Tests

The experimental images of the focal plane were taken at the LAMOST site. To verify the detection accuracy using the front-illuminated method, we also took the corresponding back-illuminated image and calculated the fiber position as a reference.

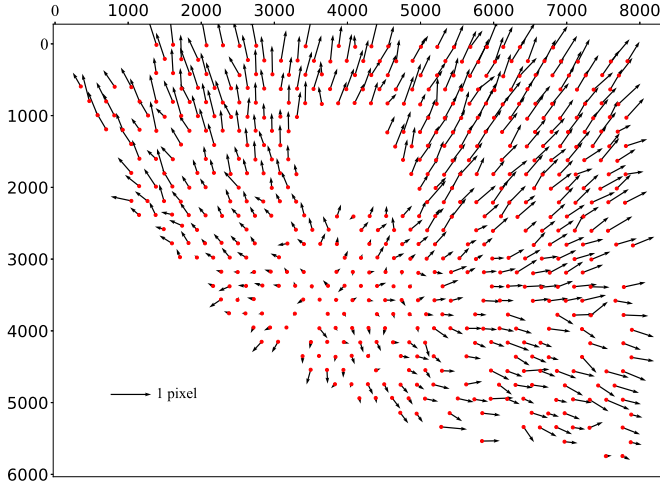


**Figure 7.** The difference in measured position between the front-illuminated method and the back-illuminated method when FPU's are at the home position. The red dots are the fiber position  $P_b$  measured by the back-illumination method, and the black arrows point to fiber position  $P_f$  measured by the front-illuminated image. The radial difference between the measurement  $P_f$  and  $P_b$  is caused by the different shooting angle between the camera and each fiber unit.

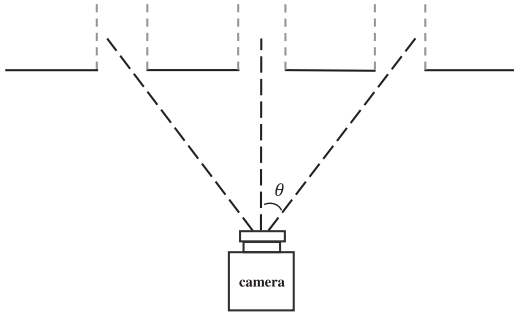


**Figure 8.** Sketch of the front-illuminated pinholes captured by the camera at different angles. When the camera is pointing toward the pinhole ( $\theta = 0$ ), the offset of position in the front-illuminated image is zero, the measurement deviation becomes larger as  $\theta$  increases.

### 3.1. Fiber Detection Accuracy

The front-illuminated image and back-illuminated image are taken almost simultaneously to avoid variation due to thermal or mechanical instability. We denote the fiber position derived from front-illuminated and back-illuminated images as  $P_f$  and  $P_b$  respectively. The difference between  $P_f$  and  $P_b$  is shown in Figure 7. As could be seen from the plot, there is a systematic variation along the radial direction between  $P_f$  and  $P_b$ . Since the front-illuminated image was taken right after the back illuminated image, the system variation due to thermal or mechanical instability should be negligible. The same test were repeated several times, each shows the similar pattern of difference between  $P_f$  and  $P_b$ , so it is not caused by the

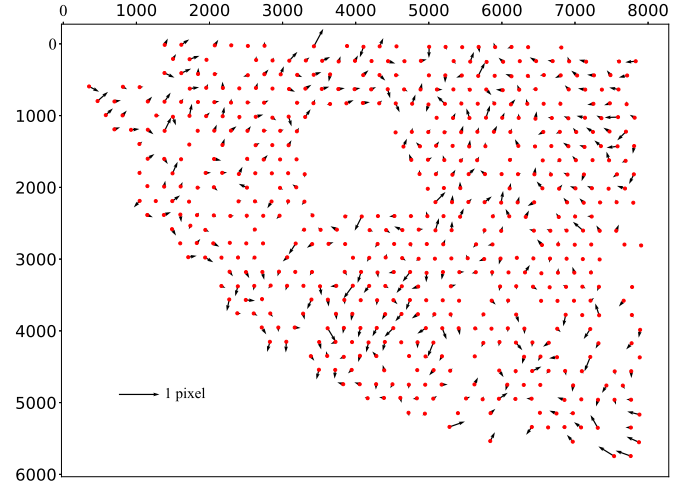


**Figure 9.** The difference in measured position between the front-illuminated method and the back-illuminated method after radial correction when FPU's are at the home position. The position offsets seen in Figure 7 are substantially eliminated.

**Table 1**

Radial Correction Parameters Calculated by the FPU's at Home Position

| $a$                   | $b$                   | $x_c$   | $y_c$   |
|-----------------------|-----------------------|---------|---------|
| $7.14 \times 10^{-2}$ | $1.20 \times 10^{-4}$ | 3604.48 | 4194.08 |

turbulence in the optical path either. Since the profile of the dark spot is determined by the light scattered inside the fiber tube then coming out in the direction of the fiber monitoring camera, so the offset between  $P_f$  and  $P_b$  is mostly determined by the front projection light and the angle between the fiber axis and the camera viewing direction (as in Figure 8). To investigate the reason for the difference, several experiments were carried out in the laboratory. The experiments show that the direction of front illumination light have minor contribution to the offset than the camera direction. As both the camera direction and the illumination light are fixed at the LAMOST site, so the pattern of the offset will not change, that means we can use the position of the back-illuminated image as a reference to correct the font-illuminated image. It should be noted that the back-illuminated image here is not necessary, it can be replaced by a certain number of fiducial fibers, a customized standard target and a certain number of reference invar rulers, etc. Assuming  $(x_c, y_c)$  is the coordinate of the intersection point that the optical axis of the camera meets the focal plane, where  $\theta$  between the pinhole of FPU and the camera is zero. The distance offset  $d$  between  $P_f$  and  $P_b$  is proportional to the angle  $\theta$  between the pinhole of the FPU and the camera optical axis. Then we can use a simple linear

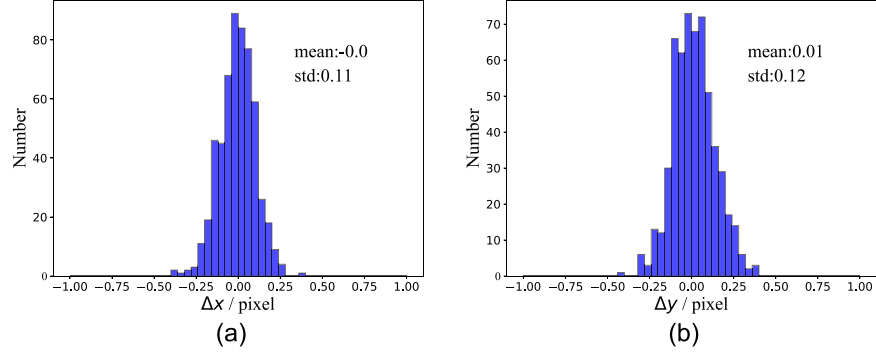


**Figure 10.** The distribution of fiber position difference between the bias corrected front-illuminated method and the back-illuminated image when the FPU are at the home position. Left for  $x$  direction and right for  $y$  direction.

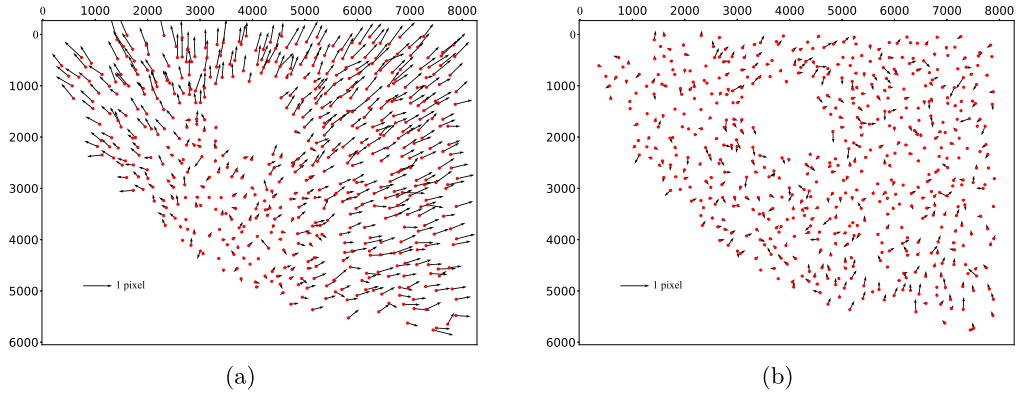


**Figure 11.** The difference in measured position between front-illuminated method and back-illuminated method when the FPU is offset from the home position. The red dots are the fiber positions measured by the back-illumination method, and the black arrows point to positions measured by the front-illuminated image. The difference before and after radial correction are shown in (a) and (b), respectively.

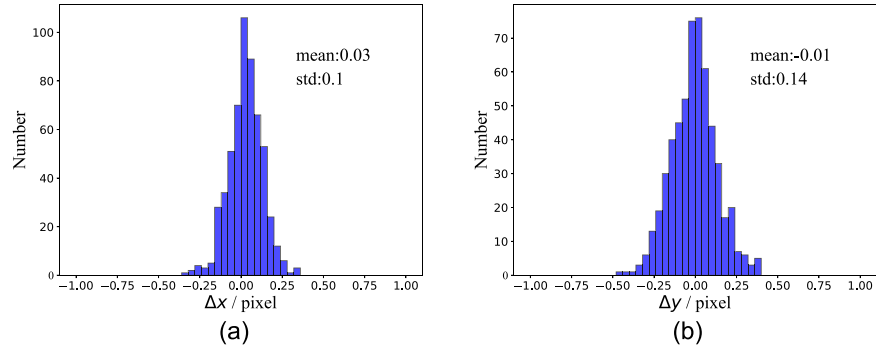


**Figure 12.** Same distribution plot as Figure 10, but for the fibers moving offset from the home position.

function to correct for the position  $P_f$ ,

$$\begin{aligned}
 d &= \sqrt{(x_f - x_b)^2 + (y_f - y_b)^2} \\
 &= a + b * \sqrt{(x_f - x_c)^2 + (y_f - y_c)^2}, \quad (3)
 \end{aligned}$$

where  $(x_f, y_f)$ ,  $(x_b, y_b)$  are the coordinates of  $P_f$  and  $P_b$  in units of pixel, respectively.  $b$  is the scaling factor, which represents the influence of the  $\theta$  on the fiber position detection. About 550 FPU are used to calculate the correction parameters, and the parameters are given in Table 1.

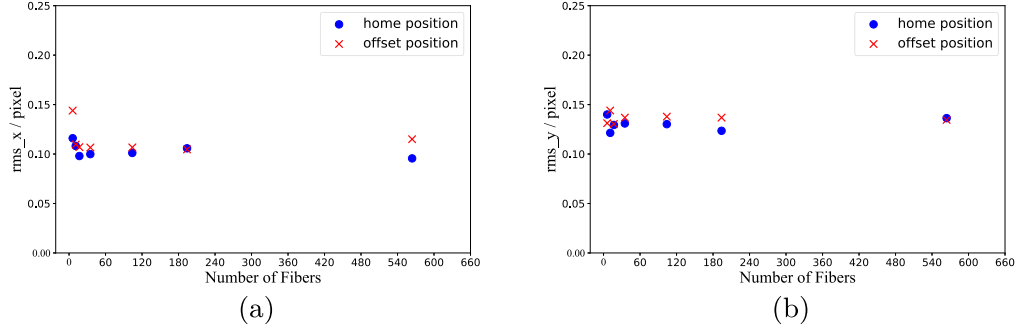


**Figure 13.** The rms of radial correction residuals vs. the number of fiber units used in deriving the correction parameters in Table 1. (a)  $x$  direction and (b)  $y$  direction. The number of FPUs has little effect on the correction parameters when it is larger than 10.

**Table 2**

Fiber Detection Accuracy of the Front-illuminated Method Compared to the Back-illuminated Method after System Correction (unit: pixel)

|      | Home Position |       | Offset Position |       |
|------|---------------|-------|-----------------|-------|
|      | rms_x         | rms_y | rms_x           | rms_y |
| 1    | 0.11          | 0.12  | 0.1             | 0.14  |
| 2    | 0.1           | 0.12  | 0.11            | 0.13  |
| 3    | 0.13          | 0.13  | 0.12            | 0.13  |
| Mean | 0.11          | 0.12  | 0.11            | 0.13  |

Applying those parameters to Equation (3), then projecting the offset  $d$  of each FPU to  $x$  and  $y$  direction respectively, we can derive the correction for each FPU. The residual distribution on the focal plane and the residuals in  $x$  and  $y$  directions are plotted in Figures 9 and 10 respectively. As the figures show, the root mean square (rms) of residual in both direction is about 0.12 pixels ( $0''.14$ ) and there is no system tendency after a simple radial correction. The position measurement precision of the front-illuminated image is comparable to the precision in the back-illuminated image, and satisfies the measurement precision requirement, which is  $0''.2$  ( $20 \mu\text{m}$ ).

The correction parameters in Table 1 are calculated by the FPUs at the home position, where the two rotation arms of the FPU stay at the initial angle (see Zhou et al. 2021a). In order to further verify the accuracy of the correction parameters, we run the FPUs to different fiber positions and correct the measurements of front illuminated image with the parameters in Table 1. The corrected results are compared with the those derived from the back-illuminated image, as shown in Figures 11 and 12. As can be seen from the figures, there is no system bias between the back-illuminated and the front-illuminated results after correction, and the residuals are similar to the previous correction results at the home position. To test the stability of the correction, the similar tests are repeated 3 times, the results are summarized in Table 2. All the rms of

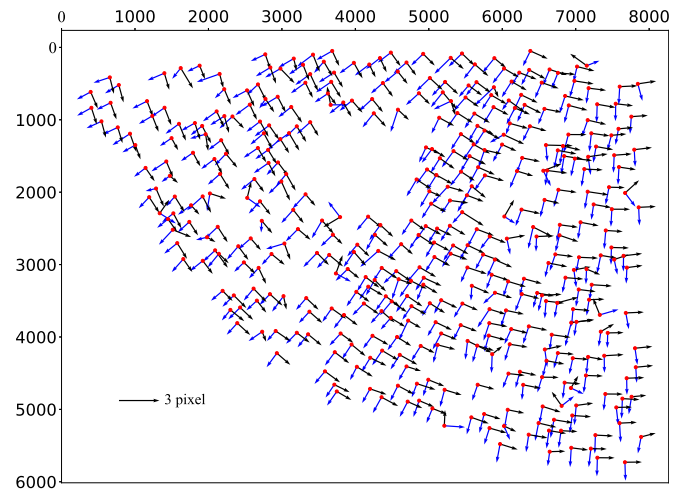


**Figure 14.** The vector diagram of two positions offset  $1''.5$  (about 1.3 pixel) away relative to the initial position. The red point is the initial position  $a$ , the blue arrow ( $ab$ ) and the black arrow ( $ac$ ) move  $1''.5$  away from position  $a$  respectively, and the two vectors are perpendicular to each other.

residual at the home position as well as the offset position are around 0.12 pixels in either direction, which indicates that after correcting the system bias of the front-illuminated image with Equation (3), we could achieve the similar detection accuracy as the back-illuminated image.

In the above experiments, we use about 550 FPUs to correct the system bias between the front-illuminated and back-illuminated images, to further reduce the calculation, we try to reduce the number of FPUs that take part in the calculation and check the corresponding correction accuracy. We sample the FPUs on the focal plane at equal intervals, and select 6, 11, 17, 35, 104, 194, and 564 FPUs respectively to calculate the correction parameters. The results show that the number of FPU has little effect on the radial correction. As shown in Figure 13, when the number of FPU is larger than 10, the difference in radial correction results is almost negligible. This

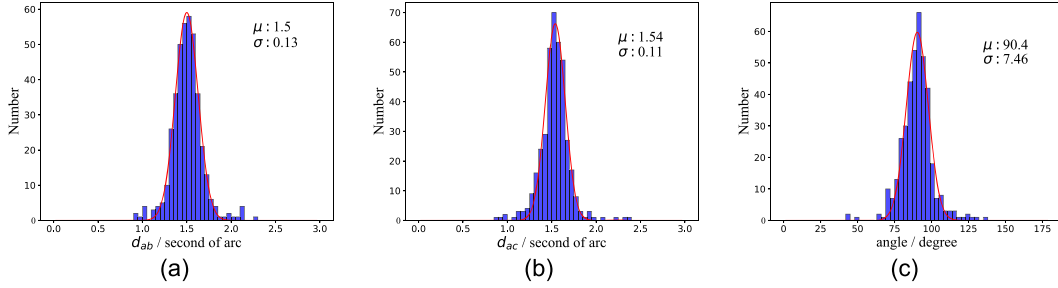


**Figure 15.** Distribution of relative distance and angle of two offset positions measured by front-illuminated method. (a) Distribution of distance  $d_{ab}$  between position  $a$  and  $b$ . (b) Distribution of  $d_{ac}$ . (c) Distribution of angle  $\angle bac$  between  $ab$  and  $ac$ .

test could be a good reference when the setting of the number of fiducial fibers for fiber detection in the closed-loop control system (Duan et al. 2020).

### 3.2. Relative Offset Test

As discussed in the previous section, the system bias between the front-illuminated and back-illuminated images are mostly caused by the direction of the camera and could be corrected by a simple linear function. For each FPU moving in a local area limited by the length of two rotation arms, the relative distance between different appointed positions should be precisely measured even without calibration by the back-illuminated image, if the front-illuminated method could reach the required accuracy.

To further verify the fiber detection accuracy of the front-illuminated method, we run the FPUs to the following three different position sets (denoted as  $a$ ,  $b$  and  $c$ , respectively): with the first position  $a$  as a reference position, the second position  $b$  moves 1.5 arcsec apart from position  $a$  with the direction along the radial direction of the focal plane and position  $c$  moves 1.5 arcsec apart from position  $a$  along the tangential direction of the focal plane, thus vector  $ab$  and  $ac$  are perpendicular to each other.

For those three fiber position sets, we take only the front-illuminated image, and calculate the position of every FPU without calibration by the back-illuminated image, the relative distance  $d_{ab}$ ,  $d_{ac}$  and the angle  $\angle bac$  between  $ab$  and  $ac$ . The vector diagram is shown in Figure 14. The distributions of  $d_{ab}$ ,  $d_{ac}$  and  $\angle bac$  are plotted in Figure 15. The distance  $d_{ab}$  and  $d_{ac}$  are both coincidence with the expected value of 1.5 arcsec with an error about 0.12 arcsec, which is consistent with the previous results. The measured angle  $\angle bac = 90.4 \pm 7^\circ$  is also consistent with the expected value. There is no obvious system bias in the vector diagram, though a few occasional failures due to mechanical error (Zhou et al. 2021a) are evidenced in Figure 14.

From the relative offset test, the accuracy of the fiber position derived from the front-illuminated image alone is

about  $0''.12$ , satisfies the demand of LAMOST fiber position measurement.

## 4. Conclusions

The closed-loop controlled fiber detection system of LAMOST is being constructed to achieve higher fiber positioning accuracy and reduce the configuration time of fiber positioning. Fiber detection is the most important part of the closed-loop control system. Unlike the back-illuminated image where only the fibers are lit up, the front-illuminated image contains all the information of the FPU, which can also be used to calculate the fiber position. We propose a new method for fiber detection based on the front-illuminated image captured by the fiber monitoring camera. The method first detects the ceramic fiber holder then derives the fiber position by fitting the profile of the pinhole inside the fiber holder with a Gaussian function. The front illuminated method shows a stable system bias when comparing with the back illuminated method, which is mostly due to the viewing angle between the FPU and the monitoring camera. As demonstrated in Section (3.1), a simple radial correction could eliminate the system bias between the two methods with precision about  $0''.14$ . Further test shows that the relative position detected using only the front illumination method is also correct with precision about  $0''.12$ , which indicates that the detection accuracy of the front-illuminated method is better than  $0''.1$ . Thus we conclude that the front-illuminated method has the same precision as the back-illuminated method and could be used in the future LAMOST closed-loop controlled fiber positioning system. The back-illuminated system would induce more overhead time and light pollution inside the spectrograph during night observations, while the method discussed in this paper would have the same accuracy with less disadvantages comparing with the back-illuminated method. Since the front-illuminated light and the monitoring camera are relative stable during each observation night, once the system correction parameters are derived before observation, the front-illuminated method could be used in the closed-loop controlled fiber positioning system with the same accuracy as the back-illuminated method.

### Acknowledgments

This work is supported by the Maintenance and renovation project of Major Science and Technology foundational facility of the Chinese Academy of Sciences, DSS-WXGZ-2020-0009 and DSS-WXGZ-2021-0004. Z.H.T. and Z.Y. also thanks the support of the National Key R&D Program of China (2019YFA0405000) and NFSC 12090041, U1931207, U2031207 and U1931126. L.J. thanks the support of the National Natural Science for Youth Foundation of China (No. 11603043). Guo Shou Jing Telescope (the Large sky Area Multi-Object fiber Spectroscopic Telescope, LAMOST) is a National Major Scientific Project built by the Chinese Academy of Sciences. Funding for the project has been provided by the National Development and Reform Commission. LAMOST is operated and managed by the National Astronomical Observatories, Chinese Academy of Sciences.

### ORCID iDs

Zengxiang Zhou  <https://orcid.org/0000-0002-3050-5822>

### References

- Baltay, C., Rabinowitz, D., Besuner, R., et al. 2019, *PASP*, **131**, 065001
- Cui, X. Q., Zhao, Y. H., Chu, Y. Q., et al. 2012, *RAA*, **12**, 1197
- Drass, H., Vanzi, L., Torres-Torriti, M., et al. 2016, *Proc. SPIE*, **9908**, 99088E
- Duan, R.-l., Li, Q.-x., Li, Y.-h., et al. 2005, *Optical Technique*, **31**, 415
- Duan, S., Zuo, J., Li, M., et al. 2020, *Proc. SPIE*, **11445**, 114456B
- Fisher, C., Morantz, C., Braun, D., et al. 2014, *Proc. SPIE*, **9151**, 91511Y
- Hörler, P., Kronig, L., Kneib, J., et al. 2018, *MNRAS*, **481**, 3070
- Liu, Z., Zhai, C., Hu, H., Wang, J., & Chu, J. 2011, *Proc. SPIE*, **8149**, 81490H
- Montgomery, D., Atkinson, D., Beard, S., et al. 2016, *Proc. SPIE*, **9908**, 990895
- Schubnell, M., Ameel, J., Besuner, R. W., et al. 2016, *Proc. SPIE*, **9908**, 990892
- Shortis, M. R., Clarke, T. A., & Short, T. 1994, *Proc. SPIE*, **2350**, 239
- Wang, S.-Y., Chou, R. C., Huang, P.-J., et al. 2016, *Proc. SPIE*, **9908**, 990881
- Xing, X., Zhai, C., Du, H., et al. 1998, *Proc. SPIE*, **3352**, 839
- Zhao, K., Liu, Z., Hu, H., et al. 2018, *Proc. SPIE*, **10700**, 107002A
- Zhou, M., Lv, G., Li, J., et al. 2021a, *PASP*, **133**, 115001
- Zhou, Z., Duan, S., Zuo, J., et al. 2021b, *JATIS*, **7**, 014007
- Zhu, G.-y., & Zhang, R.-l. 2008, *Computer Engineering and Design*, **29**, 1462